

RESEARCH ARTICLE

Open Access



# Origin, evolution, and tissue-specific functions of the porcine repetitive element 1

Min Zheng\*, Tianfu Guo, Bin Yang, Zhiyan Zhang\* and Lusheng Huang\*

## Abstract

**Background:** The porcine repetitive element 1 (PRE1) is the most abundant short interspersed nuclear element (SINE) in the *Sus scrofa* genome and it has been suggested that some PRE1 can have regulatory functions. The million copies of PRE1 in the porcine genome have accumulated abundant CpG dinucleotides and unique structural variations, such as direct repeats and patterns of sequence degeneration. The aims of this study were to analyse these structural variations to trace the origin and evolutionary pattern of PRE1 and to investigate potential methylation-related functions of PRE1 based on methylation patterns of PRE1 CpG dinucleotides in different tissues.

**Results:** We investigated the evolutionary trajectory of PRE1 and found that PRE1 originated from the ancestral CHRS-S1 family through three main successive partial duplications. We found that the partial duplications and deletions of PRE1 were likely due to RNA splicing events during retrotransposition. Functionally, correlation analysis showed that the methylation levels of 103 and 261 proximal PRE1 were, respectively, negatively and positively correlated with the expression levels of neighboring genes (Spearman correlation,  $P < 0.01$ ). Further epigenomic analysis revealed that, in the testis, demethylation of proximal PRE1 in the *HORMAD1* and *HACD3* genes had tissue-specific enhancer and promoter functions, while in the muscle, methylation of proximal PRE1 repeats in the *TCEA3* gene had an enhancer function.

**Conclusions:** The characteristic sequences of PRE1 reflect unique patterns of origin and evolution and provide a structural basis for diverse regulatory functions.

## Background

Transposable elements (TEs) constitute more than 40% of the *Sus scrofa* genome [1–3]. They have been increasingly considered to be important genomic elements for organizing genome architecture, regulating gene expression, and affecting genome size, diversity, and evolution. Comparative genomics analysis has shown that TEs are extensively co-opted for the regulation of host genes [4]. Human and animal model studies have clarified that TEs act as *cis*-regulatory elements to regulate gene expression [4–9]. They often play cell- and species/clade-specific

*cis*-regulatory roles in the modulation of gene expression through diverse mechanisms [10].

Short interspersed nuclear elements (SINEs) are retrotransposons with a high GC content and thus represent DNA methylation hotspots that can have major effects on the transcription of neighboring genes [11]. Tissue culture models have provided mounting evidence for the target-specific action of 5-methylcytosine (5mC) [12]. The methylation of SINEs or Alu elements is a highly dynamic process during human development and ageing. Methylation and demethylation of proximal Alu elements can regulate the expression of neighboring genes. For instance, hypermethylated Alu elements in the promoter of the *MIEN1* gene leads to the inhibition of its expression [13].

\*Correspondence: zhengmin@jxau.edu.cn; bioducklily@hotmail.com; lushenghuang@hotmail.com

State Key Laboratory for Pig Genetic Improvement and Production Technology, Jiangxi Agricultural University, Nanchang, China



In recent years, researchers have attempted to identify and characterize SINEs in pigs. Porcine repetitive element 1 (PRE1) accounts for 88.5% of the TEs in the pig genome, with more than one million copies [14]. PRE1 belongs to the tRNA-derived *suiform*-specific SINEs [15–17] and diversification of its sequence occurred at least 43.2 million years ago [18]. A typical PRE1 element consists of three distinct parts: the head, the body, and the tail [17]. The head contains bipartite elements of the RNA polymerase III promoter (A-box and B-box), the body harbours two short direct repeats, and the tail consists of a poly(A) tail of variable length [15]. It has been suggested that PRE1 originated from a type of SINEs called CHRS in the Suina lineage (CHRS-S) (the CHRS family of SINEs derived from tRNA<sup>Glu</sup> in a common ancestor of the lineages of *Cetaceans*, *Hippopotamuses*, *Ruminants* and *Suiformes*) [19] and then expanded through three successive events during the first half of the Tertiary period [16], including insertion of a tRNA<sup>Arg</sup>-related sequence, insertion of a 19-bp sequence, and duplication of a 28-bp sequence [20]. The expanded PRE1 elements are grouped into 15 types or lineages (Pre0\_SS, PRE1\_SS, PRE1a, b, c, d, d2, e, f, f2, g, h, i, j, and k) [14], most of which are inactive, with only PRE1a (3%) showing a weak activity [16].

Although the structure of the different PRE1 elements is clear, little is known about their evolution and biological functions. In this study, our aims were to: (1) reconstruct the evolutionary history of the PRE1 elements; (2) clarify their functions by investigating the methylation pattern of proximal PRE1 in the muscle and the testis using high-depth whole-genome bisulfite sequencing (WGBS); and (3) to attempt to identify *cis*-regulatory functions of PRE1 by combining RNA-seq and ChIP-seq data for differentially-methylated regions.

## Methods

### Animals and samples

*Longissimus dorsi* and testis tissues from eight adult male Bamaxiang pigs were used in this study. Feeding conditions and sampling methods were as described in Zheng et al. [21]. All procedures involving animals were in compliance with the guidelines for the care and use of experimental animals established by the Ministry of Agriculture of China, and the trial was approved by the Animal Ethics Committee at Jiangxi Agricultural University (No. JXAULL-2016001).

### Whole-genome bisulfite sequencing and RNA-seq

Sixteen samples from eight individuals were subjected to WGBS and RNA-seq following the standard procedures. After quality control (reads quality > Q20), the WGBS data were aligned to the *Sus scrofa* 11.1 genome assembly

using the bwa-meth-master algorithm with default parameters [22], and the Picard (MarkDuplicates) and SAMTools (rmdup) software were used for removal of PCR duplicates [23]. MethylDackel0.3.0 (<https://github.com/dpryan79/MethylDackel>) was used to summarize the methylation status of the sequences with mapping scores  $\geq 20$ . The RNA-seq data were mapped to the *Sus scrofa* 11.1 genome assembly with the HISAT2.1.0 program [24], then the StringTie software [24] was used to assemble the reads into merged transcripts, and the FeatureCounts software to quantify gene expression levels [25]. The expression levels of each transcript were quantified as fragments per kb of transcript per million mapped reads (FPKM). The raw WGBS and RNA-seq reads are deposited in the China National Center for Bioinformatics database (PRJCA003221, <https://bigd.big.ac.cn/>). The ongoing Functional Annotation of Animal Genomes (FAANG) Project shared the unpublished regional Bam files from ChIP-seq [26], miRNA-seq and Iso-seq. Mapping depth was extracted using SAMtools [27] and visualized with the Integrative Genomics Viewer (IGV) tool [28].

### Calibration and PRE1 annotation

PRE1 lineage consensus sequences were extracted from the SINEBase database (<http://sines.eimb.ru/>) [17]. To determine the length of the head–body consensus sequence for PRE1, 1000 copies of PRE1 were identified from *Sus scrofa* 11.1 by using RepeatMasker (<http://genome.ucsc.edu/>) and compared. The consensus sequence (231 nt) was then mapped to *Sus scrofa* 11.1 by BLASTn [29] to detect all the copies of PRE1 in the porcine genome.

The following step-wise approach was used to calibrate the exact coordinates of the PRE1 and to search their target site duplications (TSD). First, we extracted a ~600-nt sequence, including a ~200-nt aligned PRE1 element and a 200-nt sequence on each side. Second, we took a continuous k-mer of 8 nt from PRE1 to map the start position to the 5' end, and mapped the k-mers to the 200-nt 3' end sequence until an exact match. Third, the mapped k-mer was extended until a mismatch was identified, and the longest mapped k-mer was considered as a TSD. The distance between the two TSD was considered to be the length of the PRE1. Fourth, we used the AAAA sequence to distinguish the head–body part from the tail part of the PRE1. If no TSD was identified in the target sequence, we used the conservative GGAGTTCCC and poly(A) sequences to determine the length of the head–body part. Finally, we annotated the calibrated PRE1 based on *Sus scrofa*. *Sscrofa11.1.98.gtf*. Distances from the midpoints of the intergenic PRE1 to their neighbouring genes were

also calculated. Proximal PRE1 and distal PRE1 were defined as those that were 1 to 2 kb and 2 to 100 kb upstream of their flanking genes, respectively.

### Sequence analysis

We used the MEGA7 software [30] to perform multiple sequence alignment. Obvious alignment errors were corrected manually. Neighbour-joining trees were built using MEGA7. The nucleotide diversity and base change per site between two sequences ( $D$ ) were calculated using DnaSP6 [31]. The secondary structures of PRE1 RNA were predicted using the mfold web server (<http://unafold.rna.albany.edu/?q=mfold>) [32]. We estimated differentiation times following Nei's function ( $t = D/2\alpha$ ), with  $\alpha = 4.6 \times 10^{-9}$  [33].

The *Needleman–Wunsch* genetic distances between homologous PRE1 sequences were calculated using a custom Python script. The genetic distance matrix among sequences was used as the input data for a principal component analysis (PCA), using the PCA function from the FactoMineR R-package [34]. Results were visualized using the ggplot2 R-package [35].

The sequences of human tRNA and SINES were obtained from Vassetzky and Kramerov [17]. Six *Suidae* genome resequencing datasets were downloaded from public databases under accession numbers ERP001813 [16] and SRA096093 [36], and the reads was mapped to the *Sus scrofa* 11.1 genome assembly, using bwa [22]. We used SAMtools [27] to extract the mapping depth and IGV as the genome browser.

### Enrichment analysis of splicing signals on PRE1

First, we annotated all the calibrated PRE1 based on known exon information and selected the PRE1 that partially overlapped with the exons. Second, PRE1 overlapping with 3' UTR, 5' UTR, or RNA gene sequences were filtered out, and the sequences of PRE1 that overlapped with coding DNA sequences (CDS) of the reference genome were extracted. Third, we marked the splicing sites on PRE1. Finally, we summarized the distribution of splice sites on the consensus sequence of PRE1 by multiple sequence alignment and manual correction. We obtained 188 splicing signals in the 92-bp direct repeat region of PRE1. Hot splicing sites were defined as having at least six splicing signals at one site on the consensus sequence. The threshold was calculated by 10,000 random samplings using the sample function from the base R-package by setting  $x = 1:93$ ,  $size = 188$ , and  $replace = True$ . This resulted in a probability of 0.01 of having more than six splicing signals at one site, which was used as the significance threshold.

### Differential analysis

CpG with a read depth less than 10 and more than 300 and CpG with individual missing rates higher than 50% were filtered out. Then, we calculated the average methylation level for each CpG and gene within the filtered dataset. The Wilcoxon signed rank test was used for the differential analysis between muscle and testis tissues, using a significance threshold of 0.01. We further filtered the differentially methylated PRE1 based on previously reported differentially-methylated regions (DMR) between muscle and testis tissues [21].

## Results

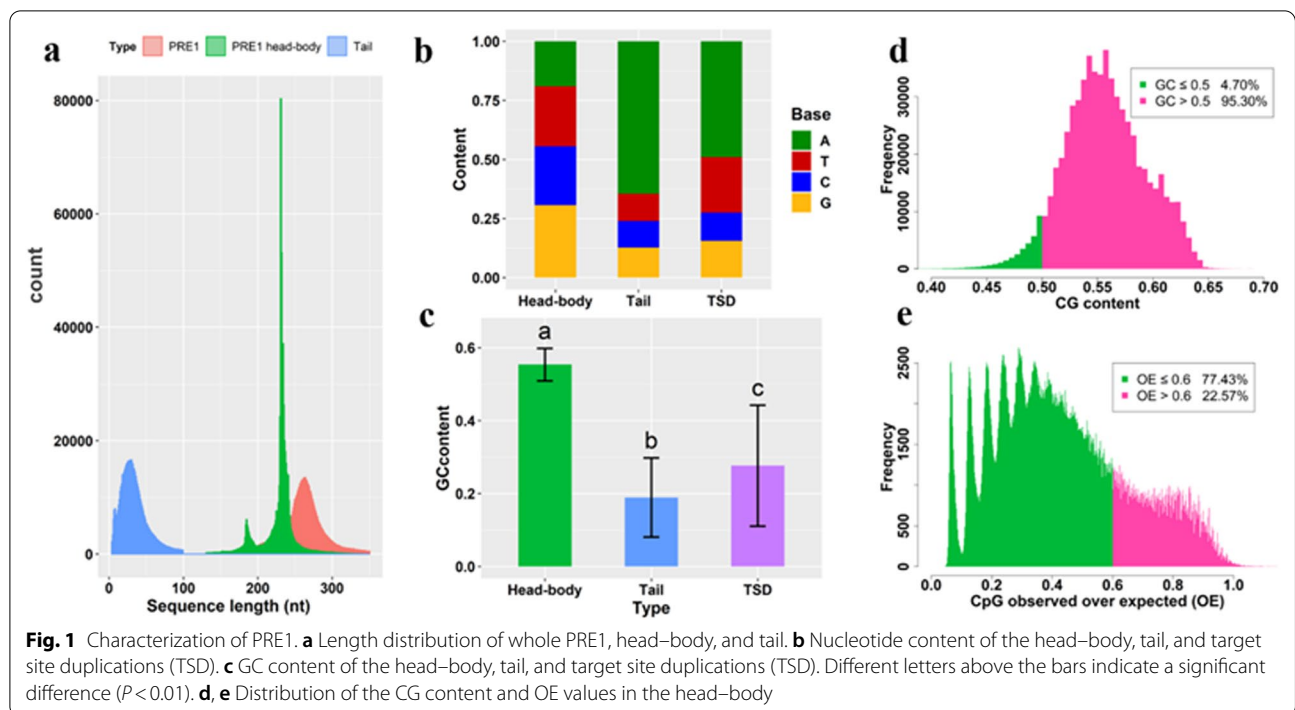
### Characterization of PRE1

Although PRE1 have been fully annotated and imported into three main databases (NCBI, Ensembl, and UCSC), their physical locations and local sequence features are not accurately annotated. Here, we recalibrated 626,582 PRE1 and their TSD. Our results show that the average full length of PRE1 was  $\sim 264$  bp, with the distribution of the head–body lengths centered mainly at 231 bp (class I) and 185 bp (class II), and the variable length of the A-rich tail ranging from 10 to 50 bp (Fig. 1a). We also detected tandem PRE1 and nested PRE1 (a PRE1 inserted into another PRE1) (see Additional file 1: Fig. S1a–d), and we observed that target site duplications were present at both ends of tandem PRE1, which suggests that part of the nested or tandem PRE1 may undergo transposition into a new genomic position (see Additional file 1: Fig. S1e). The results indicate that PRE1 have accumulated many indels and structural variations.

The three regions of PRE1 (head–body, tail, and TSD) have different nucleotide contents (Fig. 1b). The GC content in the head–body region of PRE1 (0.56) was approximately twice that in the tail (0.19) and in the TSD (0.28) (Fig. 1c, d,  $CV = 0.07$ ). In addition, 22% of the head–body sequences exhibited observed/expected CpG (OE) values above 0.6 (Fig. 1e). These results suggest that approximately 235,000 PRE1 may act as potential CpG islands on the basis of the following criteria: a minimum length of 200 bp, a minimum GC content of 50%, and an OE value above 0.6 [37]. In addition, we found that two known swine microRNA sequences are PRE1-derived miRNA, i.e. *ssc-miR-4331-1* (chr6:65468483–65468562 bp) and *ssc-mirR-4331-2* (chr14:132597139–132597207 bp).

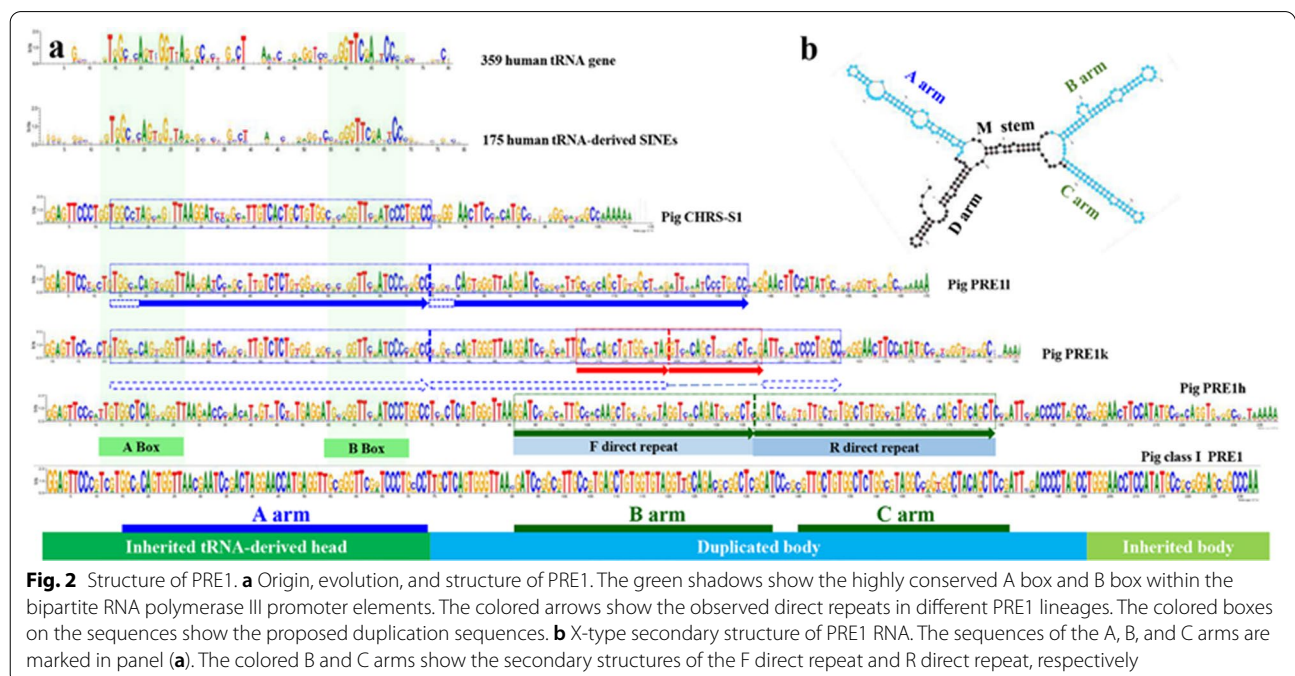
### Origin and structure of PRE1

A previous study reported that PRE1 originated from the CHRS SINE and that during the evolution of PRE1, a region homologous to tRNA<sup>Arg</sup> was inserted into its head region [20]. However, our analysis found that sequences in the head region are aligned with the head regions



(RNA polymerase III promoter) of pig CHRS-1, human tRNA-derived SINE, and human tRNA genes (Fig. 2a, green shadow), which implies that the head region of PRE1 is inherited from CHRS-S1. Thus, the previous assumption that a tRNA<sup>Arg</sup>-related sequence is inserted into the CHRS head is probably incorrect [20].

To clarify the origin of PRE1, we reconstructed its evolution by comparing the consensus sequences between different porcine PRE1 lineages and pig, bovine and caprine CHRS, which showed the presence of repetitive conserved motifs in PRE1k. Then, we carefully compared the conserved motifs to the original CHRS-S1 sequence



to uncover their origin. Importantly, this analysis suggested that two partial duplication events occurred to generate PRE1k from CHRS-S1 (Fig. 2a, blue dotted arrows and red arrows in PRE1k) and that a transitional subtype must have occurred between CHRS-S1 and PRE1k. Based on this hypothesis and sequence length data, we successfully identified this transitional subtype in the reference genome and named it PRE1l (Fig. 2a). The observed sequence signatures suggest that these two partial duplication events occurred during the evolution from CHRS-S1 to PRE1k, i.e. a duplication of an approximately 60-bp sequence of CHRS-S1 resulting in PRE1l (Fig. 2a, blue arrows in PRE1l), followed by a duplication of an approximately 18-bp sequence of the PRE1l leading to the ancestral PRE1k (Fig. 2a, red arrows in PRE1k).

Currently, class I PRE1 elements are thought to be quasi-dimeric SINEs that include two internal duplications [17]. Our results showed that there are two tandem 46-bp front (F) and rear (R) direct repeats in the body region (Fig. 2a), which updated previous knowledge of the existence of a 13-bp gap between two 34 bp direct repeats [15]. The third 46-bp duplication in the ancestral PRE1h (Fig. 2a, green arrows, F and R direct repeats) may accelerate the rate of transposition and self-evolution [14, 16]. In addition, we identified dozens of quasi-oligomeric PRE1, including three 46-bp tandem direct repeats (see Additional file 1: Fig. S2a). We also observed other internal duplications in different PRE1 (see Additional file 1: Fig. S2b). These results show that the occurrence of internal duplications has been an important mechanism for the evolution of PRE1. Further functional analysis of the duplication events showed that they seemed to be related to the X-type secondary structure of PRE1 RNA (Fig. 2b).

In summary, PRE1 originated independently from CHRS-S1 by three successive partial duplications without insertion of exogenous sequences. Molecular clock model analysis indicated that the first two duplication events occurred at least 51.6 million years ago (Mya) and the third duplication event at least 42.9 Mya, i.e. between the differentiation of *Cetartiodactyla* and the emergence of *Suiformes* [16, 19]. Based on the evolutionary tree of PRE1 (Fig. 3a) and the common structural features (head,

body, and tail) with SINEs, we conclude that PRE1 are composed of an RNA polymerase III promoter head (A box and B box), a body that is inherited from the CHR family and that includes a tRNA-related duplicated part, and a poly(A) tail (Fig. 2a, the bottom colour band).

### Splicing models for the evolution of PRE1

Another intriguing question related to the structure of PRE1 is the origin of the approximately 46-bp degenerated direct repeat in PRE1d2 and PRE1f2 (<http://sines.eimb.ru/> and (see Additional file 1: Fig. S2c) [17]; the length of the lost sequences is equal to the difference between the lengths of class I and class II PRE1 (Fig. 1a). We also detected a PRE1 element in the promoter of the *TECA3* gene [21] that had also lost a 46-bp sequence from PRE1b [chr6:81305149-81305390 bp, Fig. 3a and (see Additional file 1: Fig. S2c)]. To further investigate the presence of degenerate 46-bp sequences in the PRE1 body, we extracted all subtypes of PRE1 from class II (185 bp long without direct repeats) and constructed their evolutionary tree (Fig. 3a). The Neighbour-joining tree showed that parts of class II PRE1 and PRE1a or PRE1b are orthologous. Furthermore, we randomly extracted 10,000 PRE1 from class I and class II and calculated the *Needleman–Wunsch* genetic distances to the consensus sequences of 15 PRE1 lineages. Principal component analysis (PCA) showed that the evolutionary trajectories of these two PRE1 classes were consistent with each other (Fig. 3b), which further confirmed the orthologous relationship of class I and class II PRE1. Comparative genomic analysis revealed that the transposition activity of class II PRE1 was maintained throughout the differentiation of *Suidae* (11–2.5 Mya, Fig. 3c). Taken together, these results illustrate that the evolution of class I subtype PRE1 was accompanied by the degeneration of a 46-bp sequence in the body region.

This observation implies that a recurrent mechanism underlies the loss of a similar segment (approximately 46 bp) in the body region of class I subtype PRE1. Given that PRE1 is a retrotransposon, we analysed the sequence characteristics of PRE1 by RNA annotation. As expected, we found that a large number of PRE1 elements partially

(See figure on next page.)

**Fig. 3** The splicing model of PRE1. **a** Neighbour-joining tree based on consensus sequences of 15 PRE1 lineages, several affected PRE1, and consensus sequences of CHRS from *Sus scrofa*, *Bos taurus* and *Capra hircus*. The PRE1 shown in black font belong to class I, and those in red belong to class II. **b** Principal component analysis based on the Needleman–Wunsch genetic distance from PRE1 to the consensus sequences of 15 PRE1 lineages. Red and black dot sets represent class I and class II PRE1, respectively. The small image at the bottom left shows the specular mapping ( $x = 1$ ) of class I PRE1. **c** IGV window of the promoter region of the *TECA3* gene. The green box shows the PRE1 region in *Sus scrofa*. The six resequencing reads data downloaded from public databases, *Sus barbatus* (ERR173177) [16], *Sus cebifrons* (ERR173209) [16], *Sus celebensis* (ERR173210) [16], *Sus verrucosus* (ERR173211) [16], *Phacochoerus africanus* (ERR173203) [16], *Sus scrofa* (11-146,206) [36]. **d** Number of PRE1 that overlap with known exons. **e** Splicing signals are enriched in direct repeats. The x axis represents the base position on the consensus sequence. The font colour indicates the type of splicing signal, the physical locations of the splicing signals, and the transcript names. Numbers 3 and 5 represent the 3' splicing signal and 5' splicing signal in PRE1, respectively, and T represents the 3' splicing signal in the reverse complementary sequence of PRE1. **f** Splicing model for the PRE1 body and degenerate sequences

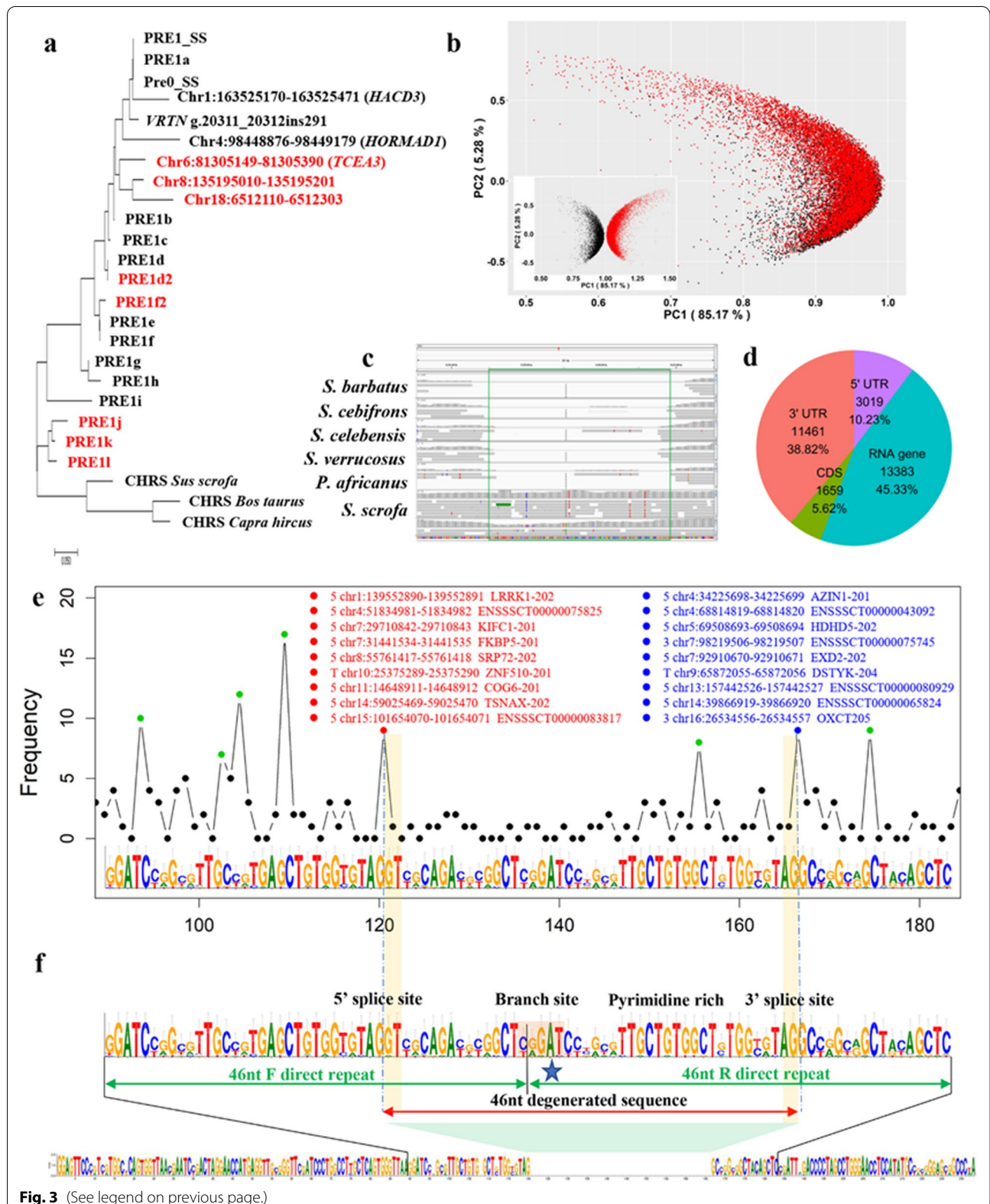


**Fig. 3** (See legend on previous page.)

overlapped with known exons, which indicates that PRE1 sequences carry splicing sites (Fig. 3d). Furthermore, we found that the splicing sites were enriched in the F and R direct repeat regions (Fig. 3e, “Methods” section). Each direct repeat carries an AG|GU splice site (Fig. 3e), which is noteworthy, as it can be used as both a 5' end and a 3' end splice site. This implies that a splicing event can potentially occur between the two dual-function splicing sites in the posttranscriptional PRE1 body. Furthermore, a branch site was found in the junction region of two direct repeats (Fig. 3f), which is similar to CTGAT in humans and mice [38–40]. Therefore, we hypothesize that the missing 46 bp between the two dual-function splicing sites were eliminated during posttranscriptional processing following the GU-AG rule (Fig. 3f), after which the processed PRE1 were reinserted into the genome by retrotransposition.

According to this splicing model, the preserved repeat sequences actually represent a chimaera of F and R direct repeats of the parental PRE1, rather than the degeneration of a single direct repeat (Fig. 3f); multiple sequence alignment showed that the splicing model had the highest alignment score [e.g. PRE1d2, (see Additional file 1: Fig. S3)]. Since the missing fragment is similar to the single direct repeat, the observed sequence of the derived class II PRE1 seems to be a degenerate whole direct repeat from class I PRE1. To further verify this hypothesis, we randomly selected 500 sequences that are homologous to F or R direct repeats from class II PRE1 and selected 100 PRE1 from class I and PRE1k as control sequences. PCA results based on *Needleman–Wunsch* genetic distances between these homologous sequences were consistent with the splicing model (Fig. 4a).

The splicing model can also explain the partial duplications of PRE1, which can arise by splicing of the post-transcriptional tandem PRE1 to form a new combinatorial PRE1 element (Fig. 4b). Similarly, it is also possible to generate new PRE1 subtypes by alternative splicing (Fig. 4b). To further validate the hypothesis of the formation of partial duplications by splicing events, we analysed the evolutionary relation of the three tandem direct repeats (repeats A, B, and C) of 82 quasi-oligomeric PRE1 (see Additional file 1: Fig. S2a). The PCA results showed that repeat C was independent from repeats A and B and that the genetic distances between repeats A and B were shorter than those between repeats B and C (Fig. 4c). To analyze the genetic relationships between the three repeats, we identified five PRE1 which shared very similar repeat A sequences but had fairly distinct B and C repeats (Fig. 4c). The results showed that the quasi-oligomeric PRE1 did not originate from the same ancestor and that the three duplication sequences did not originate from a single PRE1. The nucleotide diversity ( $\pi$ )

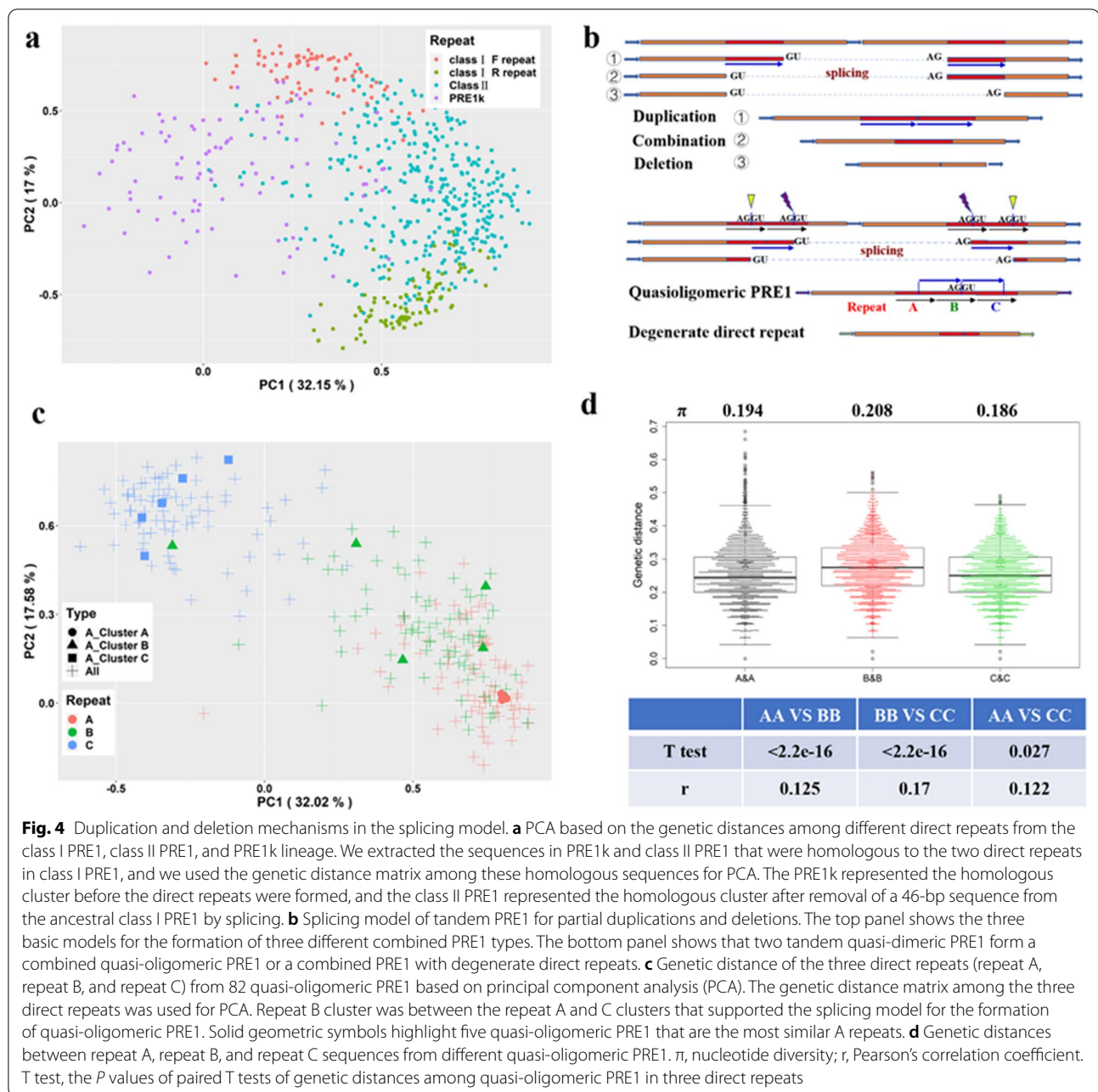
of the repeat B cluster was higher than that of the other two clusters, and the relationships within the cluster of B repeats were significantly stronger than those within the clusters of A or C repeats (paired T test,  $P < 2.2 \times 10^{-16}$ , Fig. 4d). We speculate that the B repeats are combinatorial repeats and further propose a splicing-based mechanism for the possible formation of quasi-oligomeric PRE1 (Fig. 4b, bottom).

#### Methylation level of proximal PRE1

The multiple partial duplications of tRNA-related promoter sequences and the abundant CG dinucleotides imply that PRE1 include many regulatory elements. Moreover, at least one copy of PRE1 was located 2 kb upstream for one-third of the genes and PRE1 have accumulated many variations (1000 randomly selected copies, nucleotide diversity  $\pi = 0.136$ ). Thus, PRE1 provide potential *cis*-regulatory elements.

To investigate the potential functions of PRE1, we scanned the average methylation level of CpG for 6124 PRE1 that are proximal to genes. Most of the proximal PRE1 maintained their hypermethylation in the two tissues examined, i.e. muscle and testis (Fig. 5a), and PCA showed that the methylation patterns of these PRE1 differed between the two tissues (Fig. 5b). The average methylation level was lower in the testis than in the muscle (deviation from mean = 2.40, T test,  $P < 0.05$ ) and interindividual differences were larger in the testis than in the muscle (CV 3.59 vs. 1.78%, Fig. 5c). Approximately 1128 (18.4%) PRE1 that were located proximal to 1040 genes showed significant differences in methylation level between the two tissues (Wilcoxon signed rank test,  $P < 0.01$ ), and among these genes, 247 also showed significant differential expression between these two tissues (Wilcoxon signed rank test,  $P < 0.01$ , Fig. 5d). Correlation analysis showed that the methylation level of 103 and 261 PRE1 were, respectively, negatively and positively correlated with gene expression (Spearman correlation,  $P < 0.01$ ).

To demonstrate the effect of methylated PRE1 on tissue-specific regulation, we focused on the promoter region of *TCEA3* that harbors a significantly differentially methylated PRE1 between muscle and testis (Fig. 6a) and which we had previously shown to have a methylation level that was significantly positively correlated with gene expression [21]. H3K27ac signals (Fig. 6b) showed that the differentially methylated PRE1 is located on the distal side of the enhancer of the *TCEA3* gene [41]. To exclude the possibility that the H3K27ac active signal of *TCEA3* is due to interference with the transcriptional activity of PRE1 itself, we examined the RNA-seq, small RNA-seq and Iso-seq data of adult testis and muscle tissues to check the transcriptional activity of PRE1 and found that



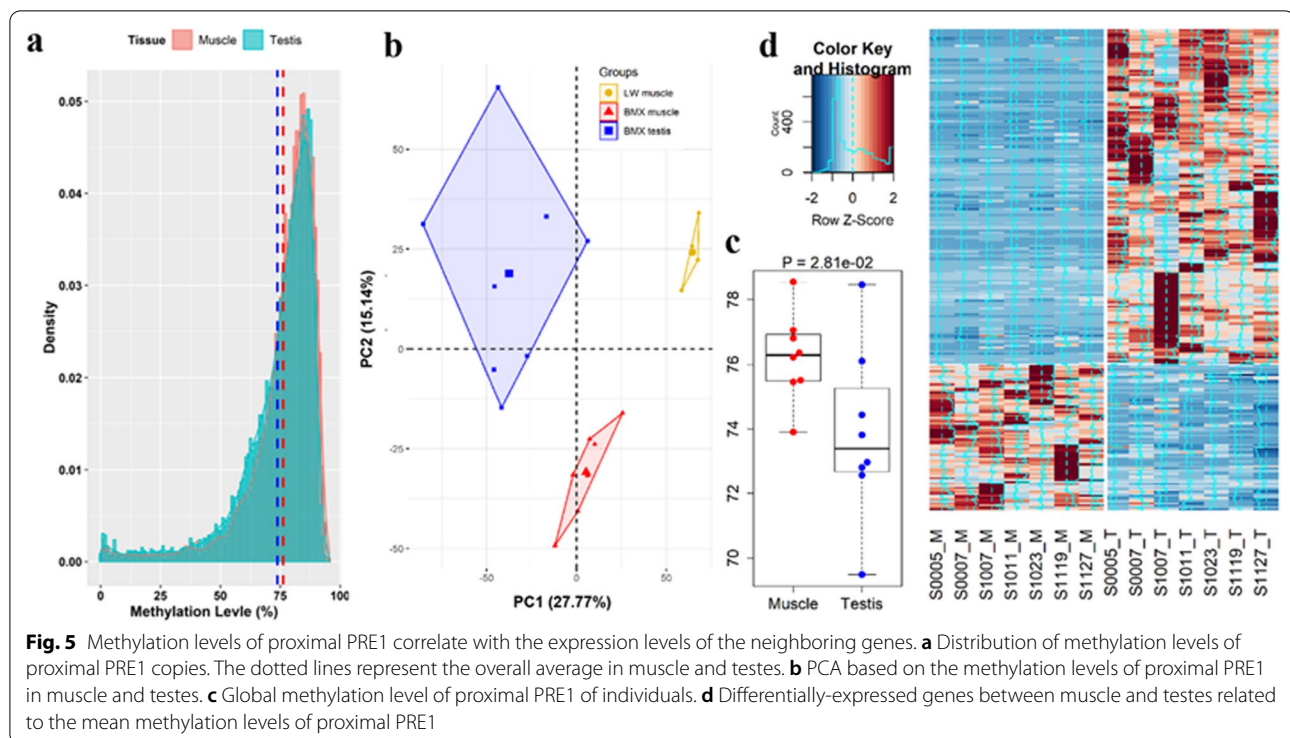
PRE1 was transcriptionally inactivated (in-house data) and no H3K4me3 peak was detected in the PRE1 regions. These results suggest that tissue-specific methylation of the *TCEA3* proximal PRE1 was conducive to enhancer-promoter activity. In addition, we observed demethylation of PRE1 in the proximal upstream regions of the *HACD3* (chr1:163525170-163525471) and *HORMAD1* (chr4:98448876-98449179) genes, which suggests a tissue-specific enhancer and promoter function [Fig. 6c, d and (see Additional file 1: Fig. S4)]. These results imply

that methylation of PRE1 is related to multiple tissue-specific *cis*-regulatory functions.

Our previous studies showed that a PRE1 copy inserted into the *VRTN* gene (*g.20311\_20312ins291*) can increase its expression nine-fold in pig embryos and can also increase the number of thoracic vertebrae [9, 42, 43]. Moreover, PRE1 activates the expression of reporter genes, both in vitro and in vivo [9].

According to a previous analysis of an intragenic PRE1 (*VRTN g.20311\_20312ins291*) that promotes host gene





transcription [9], most enhancers are enriched in regions that are 2 to 100 kb away from the nearest gene [44–46]. We compared the differentially-methylated PRE1 in the intragenic, proximal, and distal regions. The numbers of PRE1 in these three regions are shown in Fig. 6e. We captured the differentially-methylated PRE1 between muscle and testis by setting stricter criteria, including at least 10 filtered CpG in each PRE1 copy, a Wilcoxon signed rank test  $P < 0.01$ , and an absolute difference between the means of the two tissues greater than 0.3. The numbers of differentially-methylated PRE1 and differentially-expressed genes are shown in Fig. 6f. The results showed that, compared to other PRE1, proximal PRE1 are more likely to show differential methylation between muscle and testis (Fisher's exact test,  $P < 0.01$ ).

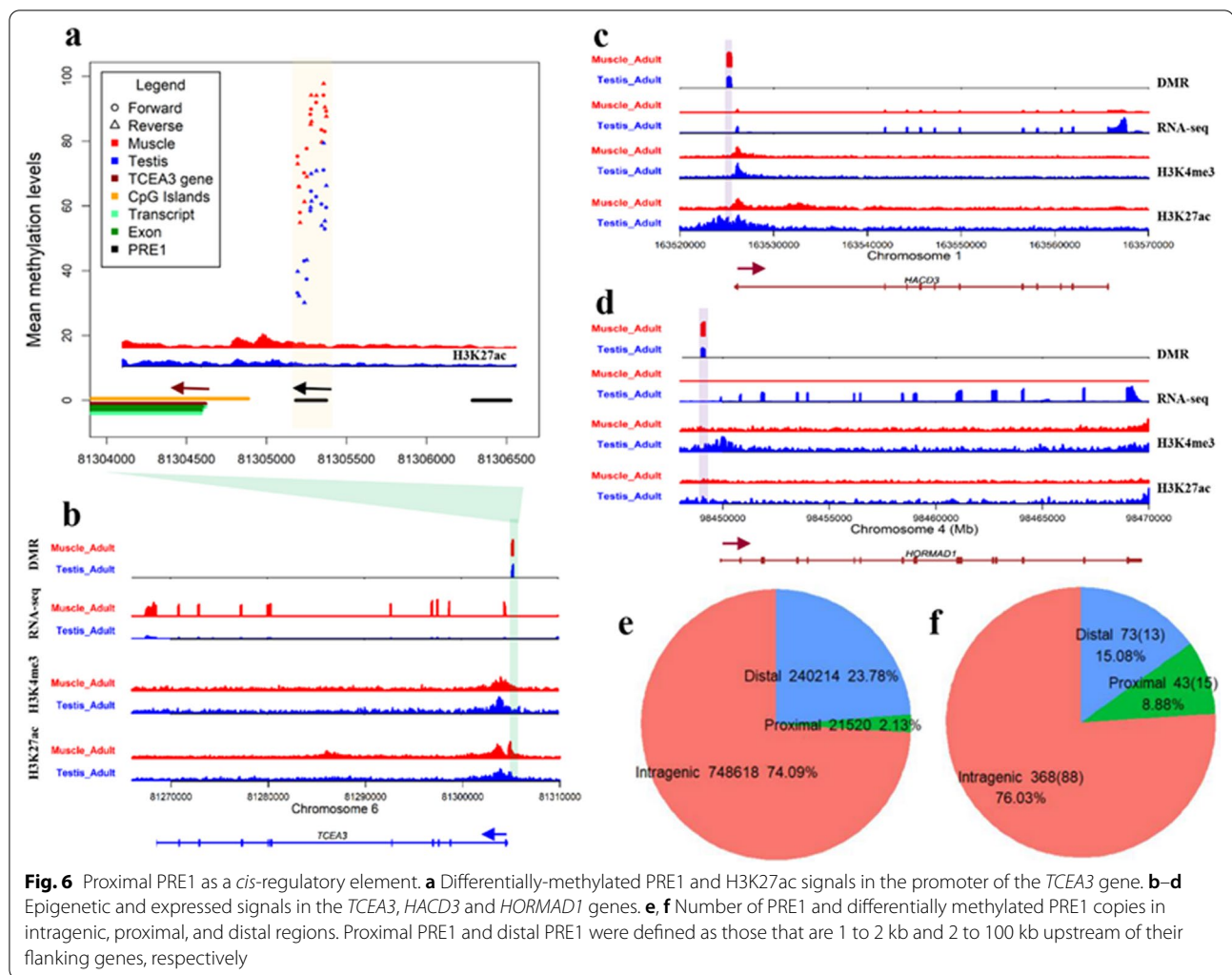
## Discussion

In this study, we modelled the evolution of the PRE1 sequence from the ancestral CHRS-S1 family to its current form through three successive partial duplications. Specifically, PRE1 RNA splicing models have been proposed to explain partial duplications, deletions, and degenerate direct repeats in PRE1. Epigenetic evidence shows that PRE1 may act as methylation-associated functional elements.

We propose to divide the PRE1 lineages into four sub-families (PRE1A, PRE1B, PRE1C, and PRE1D) based on evolutionary history, which includes three successive

partial duplications and degenerations of direct repeats. The partial duplication of the CHRS-1 head region leads to the ancestral PRE1 subfamily (PRE1A or PRE1I). A short partial duplication in the PRE1A body region forms the ancestral PRE1B (including PRE1i, PRE1j, and PRE1k). Similarly, a long partial duplication in the PRE1B body region produces the ancestral PRE1C (including PRE1a, PRE1b, PRE1c, PRE1d, PRE1e, PRE1f, PRE1h). PRE1D (including PRE1d2 and PRE1f2) is produced by degeneration of a direct repeat from PRE1C. Although we have redrawn the general structure of PRE1, it must be noted that the PRE1 family has accumulated a large number of different indels (Fig. 1a). A previous study reported that the PRE1a lineage contains elements that are similar, indicating very recent and possibly current activity [16]. Following the splicing model, the activity of PRE1a should contribute to the continuous formation of new PRE1 copies, with possible new duplication/deletion events.

The retrotransposition of PRE1 increases the length of genes and causes alternative splicing. We analyzed 21,420 single-copy genes that were longer than 1000 bp and found that the number of PRE1 was strongly correlated with gene length (Spearman's  $r = 0.912$ ,  $P < 2.2 \times 10^{-16}$ ). The PRE1 copy number was moderately correlated with the number of annotated gene transcripts (Spearman's  $r \approx 0.5$ ,  $P < 2.2 \times 10^{-16}$ ). A large number of splicing signals was detected in PRE1 (Fig. 3e). These results showed



that intragenic PRE1 may mediate alternative splicing and exonization of protein-coding genes. Strong splicing signals (GU-AG) in PRE1 provided resources for partial duplications over a long evolutionary history and is probably the phenomenon that drives complex repetitive structures in CHRS families [17]. Partial duplications and degenerations are important mechanisms for increasing the diversity and complexity of the PRE1 sequences.

SINEs are considered to be *cis*-regulatory elements [10, 47]. We used multidimensional epigenomic data to identify tissue-specific *cis*-regulatory PRE1 elements through methylation analysis of CpG in PRE1. As proof of principle, we show that three PRE1 close to the *TCEA3*, *HACD3*, and *HORMAD1* genes act as promoters or enhancers to activate or enhance gene expression by methylation. Differentially-methylated PRE1 in the muscle and testis were positively or negatively correlated with the expression of neighboring genes. This illustrates that methylated proximal PRE1 have dual

functions (inhibition and activation) in the regulation of gene expression. ChIP-seq data show that these functional PRE1 elements are located in the distal flanks of enhancers, which is consistent with the previous view that enhancers that are located on either side of SINEs could provide platforms for chromatin rearrangement via the physical or biochemical properties of their sequences [41]. The functions of PRE1 as regulatory elements can be spatiotemporally specific, and DNA methylation plays an important epigenetic function to adapt the binding to specifically expressed *trans*-acting factors and achieve specific regulating effects. CpG methylation can influence the binding affinity of most transcription factors to DNA [48]. Some of these transcription factors have two functions depending on the tissue and act as silencers and enhancers in different cellular contexts [49]. PRE1 subfamilies are enriched for specific TF motifs, and not every PRE1 can be effectively bound by those TF because of epigenetic modification, co-selection, and mutation

[10]. In conclusion, the unique origin and evolution of PRE1 provide a structural basis for diverse regulatory functions. More research is needed to identify and differentiate context-, motif- or lineage-specific functions, and multifunctional PRE1 copies.

Through this study, we summarized several features of PRE1 as diverse *cis*-regulatory elements. First, most PRE1 are inactive and have lost their transposition ability during their evolution [14, 16]. Most extant PRE1 insertions are neutral to the host gene and have become fixed through genetic drift [10]. The three partial duplications of the tRNA promotor for the PRE1 body amplified the affinity of promoter transcription factors (Fig. 2a). Thus, it naturally follows that PRE1 near the host gene may interfere with its expression. Second, some PRE1 have accumulated many CG dinucleotides (Fig. 1c, d), which can act as CpG islands to increase or decrease gene expression by methylation [48, 50, 51]. Third, the PRE1 family has evolved into abundant lineages through single nucleotide variation, insertion, deletion, and partial duplication (Figs. 1a and 2a). These different lineages might have acquired specific TF-binding motifs [10]. Finally, the million or more PRE1 in the genome can physically interact with other regulatory elements and promoters and form stable 3D structures [47].

In addition, intragenic PRE1 are involved in posttranscriptional regulation processes. First, most splicing sites are enriched in PRE1 (Fig. 3e), and PRE1 in introns of transcribed genes mediate exonization and alternative splicing. Second, we predicted that PRE1 RNA has a complex spatial structure (Fig. 2b) and that many PRE1 are proximal to the 3' and 5' UTR of genes (Fig. 3d). PRE1 in the 5' UTR of mRNA can suppress translation by forming secondary structures [52], and PRE1 in the 3' UTR can increase the stability of the mRNA. Third, we found that two miRNA (ssc-miR-4331-1 and ssc-miRNA-4331-2) are derived from PRE1 and may regulate homologous PRE1-derived target sites in the 3' UTR of the mRNA. Finally, PRE1 has other functions similar to those of the human SINEs (Alu) [47].

## Conclusions

In this study, we focused on the origin, evolution and functions of porcine PRE1. PRE1 have originated from CHRS-1 through three main partial duplications. The PRE1 family has accumulated many structural variations including duplications, deletions, insertions, and degenerate direct repeats over a long history of propagation. In particular, the late evolution of PRE1 was accompanied by the degeneration of direct repeats. We also observed many splicing sites that are located within intragenic PRE1. These splicing sites in single PRE1 and in nested and tandem PRE1 have contributed

to the evolution of PRE1. We inferred a PRE1 RNA splicing model, which may explain the formation of partial duplications and degenerate direct repeats. In terms of *cis*-regulatory functions, we found that PRE1 sequences act as methylation-associated tissue-specific enhancers or promoters.

## Supplementary Information

The online version contains supplementary material available at <https://doi.org/10.1186/s12711-022-00745-3>.

**Additional file 1: Figure S1.** Nested and tandem PRE1. **a** Mechanisms of the formation of nested PRE1 and tandem PRE1. **b** A PRE1 inserted into another PRE1 tail. The target motif is located in the PRE1 tail (chr7:29710723:29711249). The nested PRE1 are actually two new tandem PRE1 with changed tile lengths. The tail of the basal PRE1 at the 5' end is shortened, but the tail of the embedded PRE1 at the 3' end is extended. Target site duplications (TSD) are shown in red font. Embedded PRE1 are shown in blue font, and basal PRE1 are shown in green font. **c** Repeated TSD produce three tandem PRE1 (chr12:33294823-33295640); **d** A PRE1 inserted into another PRE1 body. The target motif is located in the PRE1 body, which leads to a nested PRE1 (chr14:22207023-22207668); and **e** A tandem PRE1 inserted into the genome (chr2:80470307-80470742). **Figure S2.** Internal repeat segments in PRE1. **a** The consensus sequence of quasi-oligomeric PRE1 including three direct repeats. The black arrows indicate the three direct repeats; **b** Several rare PRE1 with other direct repeats in the PRE1 body. Four repeat segments of PRE1 (chr15:28050427-28050730, chr6:166491294-166491728, chr7:65896533-65896843; and chr15:77600095-77600373) have been marked in the consensus sequence. The arrows show the duplicated segments in different PRE1; and **c** The degenerate 46-bp repeat sequence in PRE1. The blue dotted arrows show the degenerate 46-bp repeat sequence, and the green arrows show the direct repeats. **Figure S3.** Three alternative alignment methods for PRE1d2. The PRE1d2 shows a degenerate 46-bp segment following the splicing model, and PRE1d2(2) and PRE1d2(3) show hypothetically missed whole R or F direct repeats, respectively. **Figure S4.** Differentially-methylated PRE1 in the promoter regions of the *HACD3* and *HORMAD1* genes.

## Author contributions

MZ performed data analysis and wrote the manuscript. TG bred the animals and collected the tissues for methylome and transcriptome profiling. BY provided and analyzed the Chip-seq data of the three PRE1 regions. ZZ performed data analysis and revised the manuscript. LH designed and supervised the project. All authors read and approved the final manuscript.

## Funding

This work is supported by The National Key R & D Program of China (No. 2020YFA0509500) and National Natural Science Foundation of China (No. 31760656).

## Availability of data and materials

The methylation and RNA-seq data of the 16 samples (8 testes and 8 muscles) have been deposited in the China National center for Bioinformatics with project ID PRJCA003221 (<https://bigd.big.ac.cn/bioprotect/browse/PRJCA003221>).

## Declarations

### Ethics approval and consent to participate

All procedures involving animals are in compliance with guidelines for the care and use of experimental animals established by the Ministry of Agriculture of China, and the trial was approved by the Animal Ethics Committee at Jiangxi Agricultural University (No. JXAULL-2016001).

### Consent for publication

Not applicable.

**Competing interests**

The authors declare that they have no competing interests.

Received: 25 January 2022 Accepted: 4 July 2022

Published online: 27 July 2022

**References**

- Zhou R, Li ST, Yao WY, Xie CD, Chen Z, Zeng ZJ, et al. The Meishan pig genome reveals structural variation-mediated gene expression and phenotypic divergence underlying Asian pig domestication. *Mol Ecol Resour*. 2021;21:2077–92.
- Chen J, Zhong J, He X, Li X, Ni P, Safner T, et al. The de novo assembly of a European wild boar genome revealed unique patterns of chromosomal structural variations and segmental duplications. *Anim Genet*. 2022;53:281–92.
- Warr A, Affara N, Aken B, Beiki H, Bickhart DM, Billis K, et al. An improved pig reference genome sequence to enable pig genetics and genomics research. *Gigascience*. 2020;9:giaa051.
- Chuong EB, Elde NC, Feschotte C. Regulatory activities of transposable elements: from conflicts to benefits. *Nat Rev Genet*. 2016;18:71–86.
- Bejerano G, Lowe CB, Ahituv N, King B, Siepel A, Salama SR, et al. A distal enhancer and an ultraconserved exon are derived from a novel retroposon. *Nature*. 2006;441:87–90.
- Lunyak VV, Prefontaine GG, Nunez E, Cramer T, Ju B, Ohgi KA, et al. Developmentally regulated activation of a SINE B2 repeat as a domain boundary in organogenesis. *Science*. 2007;317:248–51.
- Ding Y, Berrocal A, Morita T, Longden KD, Stern DL. Natural courtship song variation caused by an intronic retroelement in an ion channel gene. *Nature*. 2016;536:329–32.
- Flemer M, Malik R, Franke V, Nejezpinska J, Sedlacek R, Vlahovicek K, et al. A retrotransposon-driven dicer isoform directs endogenous small interfering RNA production in mouse oocytes. *Cell*. 2013;155:807–16.
- Duan Y, Zhang H, Zhang Z, Gao J, Yang J, Wu Z, et al. VRTN is required for the development of thoracic vertebrae in mammals. *Int J Biol Sci*. 2018;14:667–81.
- Sundaram V, Wysocka J. Transposable elements as a potent source of diverse cis-regulatory sequences in mammalian genomes. *Philos Trans R Soc Lond B Biol Sci*. 2020;375:20190347.
- Ichiyanagi K. Epigenetic regulation of transcription and possible functions of mammalian short interspersed elements, SINEs. *Genes Genet Syst*. 2013;88:19–29.
- Deniz O, Frost JM, Branco MR. Regulation of transposable elements by DNA modifications. *Nat Rev Genet*. 2019;20:417–31.
- Rajendiran S, Gibbs LD, Van Treuren T, Klinkebiel DL, Vishwanatha JK. MIEN1 is tightly regulated by SINE Alu methylation in its promoter. *Oncotarget*. 2016;7:65307–19.
- Fang X, Mou Y, Huang Z, Li Y, Han L, Zhang Y, et al. The sequence and analysis of a Chinese pig genome. *Gigascience*. 2012;1:16.
- Singer DS, Parent LJ, Ehrlich R. Identification and DNA sequence of an interspersed repetitive DNA element in the genome of the miniature swine. *Nucleic Acids Res*. 1987;15:2780.
- Groenen MAM, Archibald A, Uenishi H, Tuggle CK, Takeuchi Y, Rothschild MF, et al. Analyses of pig genomes provide insight into porcine demography and evolution. *Nature*. 2012;491:393–8.
- Vassetzky NS, Kramerov DA. SINEBase: a database and tool for SINE analysis. *Nucleic Acids Res*. 2013;41:D83–9.
- Yasue H, Wada Y. A swine SINE (PRE-1 sequence) distribution in swine-related animal species and its phylogenetic analysis in swine genome. *Anim Genet*. 1996;27:95–8.
- Groenen MAM. A decade of pig genome sequencing: a window on pig domestication and evolution. *Genet Sel Evol*. 2016;48:23.
- Shimamura M, Abe H, Nikaido M, Ohshima K, Okada N. Genealogy of families of SINEs in cetaceans and artiodactyls: the presence of a huge superfamily of tRNA(Glu)-derived families of SINEs. *Mol Biol Evol*. 1999;16:1046–60.
- Zheng M, Xiao S, Guo T, Rao L, Li L, Zhang Z, et al. DNA methylomic homogeneity and heterogeneity in muscles and testes throughout pig adulthood. *Aging (Albany NY)*. 2020;12:25412–31.
- Li H, Durbin R. Fast and accurate short read alignment with Burrows-Wheeler transform. *Bioinformatics*. 2009;25:1754–60.
- Ebbert MT, Wadsworth ME, Staley LA, Hoyt KL, Pickett B, Miller J, et al. Evaluating the necessity of PCR duplicate removal from next-generation sequencing data and a comparison of approaches. *BMC Bioinformatics*. 2016;17(Suppl 7):239.
- Perteua M, Kim D, Perteua GM, Leek JT, Salzberg SL. Transcript-level expression analysis of RNA-seq experiments with HISAT StringTie and Ballgown. *Nat Protoc*. 2016;11:1650–67.
- Liao Y, Smyth GK, Shi W. featureCounts: an efficient general purpose program for assigning sequence reads to genomic features. *Bioinformatics*. 2014;30:923–30.
- Zhu Y, Zhou Z, Huang T, Zhang Z, Li W, Ling Z, et al. Mapping and analysis of a spatiotemporal H3K27ac and gene expression spectrum in pigs. *Sci China Life Sci*. 2022. <https://doi.org/10.1007/s11427-021-2034-5> (in press).
- Li H, Handsaker B, Wysoker A, Fennell T, Ruan J, Homer N, et al. The sequence alignment/map format and SAMtools. *Bioinformatics*. 2009;25:2078–9.
- Thorvaldsdóttir H, Robinson JT, Mesirov JP. Integrative Genomics Viewer (IGV): high-performance genomics data visualization and exploration. *Brief Bioinform*. 2013;14:178–92.
- Chen Y, Ye W, Zhang Y, Xu Y. High speed BLASTN: an accelerated MegaBLAST search tool. *Nucleic Acids Res*. 2015;43:7762–8.
- Kumar S, Stecher G, Tamura K. MEGA7: molecular evolutionary genetics analysis version 7.0 for bigger datasets. *Mol Biol Evol*. 2016;33:1870–4.
- Rozas J, Ferrer-Mata A, Sánchez-DelBarrio JC, Guirao-Rico S, Librado P, Ramos-Onsins SE, et al. DnaSP 6: DNA sequence polymorphism analysis of large data sets. *Mol Biol Evol*. 2017;34:3299–302.
- Zuker M. Mfold web server for nucleic acid folding and hybridization prediction. *Nucleic Acids Res*. 2003;31:3406–15.
- Li WH, Gojobori T, Nei M. Pseudogenes as a paradigm of neutral evolution. *Nature*. 1981;292:237–9.
- Lê SJJ, Husson F. FactoMineR: an R package for multivariate analysis. *J Stat Softw*. 2008;25:1–18.
- Ginestet C. ggplot2: elegant graphics for data analysis. *J R Stat Soc*. 2011;174:245–6.
- Ai H, Fang X, Yang B, Huang Z, Chen H, Mao L, et al. Adaptation and possible ancient interspecies introgression in pigs identified by whole-genome sequencing. *Nat Genet*. 2015;47:217–25.
- Gardiner-Garden M, Frommer M. CpG islands in vertebrate genomes. *J Mol Biol*. 1987;196:261–82.
- Keller EB, Noon WA. Intron splicing: a conserved internal signal in introns of animal pre-mRNAs. *Proc Natl Acad Sci USA*. 1984;81:7417–20.
- Will CL, Luhrmann R. Spliceosome structure and function. *Cold Spring Harb Perspect Biol*. 2011;3: a003707.
- Lee Y, Rio DC. Mechanisms and regulation of alternative pre-mRNA splicing. *Annu Rev Biochem*. 2015;84:291–323.
- Ye M, Goudot C, Hoyle T, Lemoine B, Amigorena S, Zueva E. Specific subfamilies of transposable elements contribute to different domains of T lymphocyte enhancers. *Proc Natl Acad Sci USA*. 2020;117:7905–16.
- Fan Y, Xing Y, Zhang Z, Ai H, Ouyang Z, Ouyang J, et al. A further look at porcine chromosome 7 reveals VRTN variants associated with vertebral number in Chinese and Western pigs. *PLoS One*. 2013;8: e62534.
- Yang J, Huang L, Yang M, Fan Y, Li L, Fang S, et al. Possible introgression of the VRTN mutation increasing vertebral number, carcass length and teat number from Chinese pigs into European pigs. *Sci Rep*. 2016;6:19240.
- Cao Y, Chen G, Wu G, Zhang X, McDermott J, Chen X, et al. Widespread roles of enhancer-like transposable elements in cell identity and long-range genomic interactions. *Genome Res*. 2019;29:40–52.
- Villar D, Berthelot C, Aldridge S, Rayner TF, Lukk M, Pignatelli M, et al. Enhancer evolution across 20 mammalian species. *Cell*. 2015;160:554–66.
- Oudelaar AM, Higgs DR. The relationship between genome structure and function. *Nat Rev Genet*. 2020;22:154–68.
- Chen LL, Yang L. ALU alternative regulation for gene expression. *Trends Cell Biol*. 2017;27:480–90.
- Yin Y, Morgunova E, Jolma A, Kaasinen E, Sahu B, Khund-Sayeed S, et al. Impact of cytosine methylation on DNA binding specificities of human transcription factors. *Science*. 2017;356:eaaj2239.

49. Gisselbrecht SS, Palagi A, Kurland JV, Rogers JM, Ozadam H, Zhan Y, et al. Transcriptional silencers in *Drosophila* serve a dual role as transcriptional enhancers in alternate cellular contexts. *Mol Cell*. 2020;77:324-37.e8.
50. Hartl D, Krebs AR, Grand RS, Baubec T, Isbel L, Wirbelauer C, et al. CG dinucleotides enhance promoter activity independent of DNA methylation. *Genome Res*. 2019;29:554–63.
51. Carter B, Zhao K. The epigenetic basis of cellular heterogeneity. *Nat Rev Genet*. 2021;22:235–50.
52. Sobczak K, Krzyzosiak WJ. Structural determinants of BRCA1 translational regulation. *J Biol Chem*. 2002;277:17349–58.

### **Publisher's Note**

Springer Nature remains neutral with regard to jurisdictional claims in published maps and institutional affiliations.

**Ready to submit your research? Choose BMC and benefit from:**

- fast, convenient online submission
- thorough peer review by experienced researchers in your field
- rapid publication on acceptance
- support for research data, including large and complex data types
- gold Open Access which fosters wider collaboration and increased citations
- maximum visibility for your research: over 100M website views per year

**At BMC, research is always in progress.**

Learn more [biomedcentral.com/submissions](https://biomedcentral.com/submissions)

